

Article

Not peer-reviewed version

Development and Characterization of LL37 Antimicrobial Peptide-Loaded Chitosan Nanoparticles: An Antimicrobial Sustained Release System

[Fazilet CANATAN ERGÜN](#)^{*}, [Meltem DEMİREL KARS](#)^{*}, [Gökhan KARS](#)^{*}

Posted Date: 26 May 2025

doi: 10.20944/preprints202505.1937.v1

Keywords: chitosan; LL37; nanoparticle; ionic gelation; drug release kinetics; biocompatibility; antibacterial



Preprints.org is a free multidisciplinary platform providing preprint service that is dedicated to making early versions of research outputs permanently available and citable. Preprints posted at Preprints.org appear in Web of Science, Crossref, Google Scholar, Scilit, Europe PMC.

Copyright: This open access article is published under a Creative Commons CC BY 4.0 license, which permit the free download, distribution, and reuse, provided that the author and preprint are cited in any reuse.

Article

Development and Characterization of LL37 Antimicrobial Peptide-Loaded Chitosan Nanoparticles: An Antimicrobial Sustained Release System

Fazilet Canatan Ergün ^{1,*}, Meltem Demirel Kars ¹ and Gökhan Kars ²

¹ Department of Biomedical Engineering, Faculty of Engineering, Necmettin Erbakan University, Konya 42140, Turkey

² Department of Molecular Biology and Genetics, Faculty of Science, Necmettin Erbakan University, Konya 42140, Turkey

* Correspondence: fzelt.cntrn93@gmail.com

Abstract: CSNPs synthesized via the ionic gelation method, have emerged as a promising nanoplatform in diverse fields such as pharmaceuticals, nanotechnology, and polymer science due to their biocompatibility, ease of fabrication, and tunable properties. Their nanoscale dimensions are critical in modulating drug loading efficiency, release kinetics, and interactions with biological environments. This study focuses on the development and characterization of LL37-loaded CSNPs, designed to enhance antibacterial efficacy while maintaining biocompatibility. To achieve this, CSNPs were optimized for size and stability by adjusting parameters such as chitosan concentration, pH, and stabilizer. LL37, a potent antimicrobial peptide, was successfully encapsulated into CSNPs at concentrations of 7.5, 15 and 30 µg/mL, yielding formulations with favorable physicochemical properties. Dynamic light scattering (DLS) and Zeta sizer analyses revealed that blank CSNPs exhibited an average particle size of 180.40 ± 2.16 nm, a zeta potential (ZP) of $+40.57 \pm 1.82$ mV, and a polydispersity index (PDI) of 0.289. In contrast, 15-LL37-CSNPs demonstrated an increased size of 210.9 ± 2.59 nm with an enhanced zeta potential of $+51.21 \pm 0.93$ mV, indicating improved stability and interaction potential. Field emission scanning electron microscopy (FE-SEM) analyses exhibited the morphology of nanoparticles, demonstrating the round shaped CSNPs. The release profile of LL37 exhibited a concentration-dependent rate and showed the best fit with the first-order kinetic model. This indicates that the release rate is proportional to the remaining amount of LL37 in the formulation. Cytocompatibility assessments using the XTT assay confirmed that both blank and LL37-loaded CSNPs did not exhibit cytotoxicity on HS2-keratinocyte cells across a range of concentrations (150 µg/mL to 0.29 µg/mL). Notably, LL37-loaded CSNPs demonstrated significant antibacterial activity against *E. coli* and *S. aureus*, with the 15-LL37-CSNP formulation exhibiting superior efficacy. Overall, these findings highlight the potential of LL37-CSNPs as a versatile antibacterial delivery system with applications in drug delivery, wound healing, and tissue engineering.

Keywords: chitosan; LL37; nanoparticle; ionic gelation; drug release kinetics; biocompatibility; antibacterial

1. Introduction

Nanotechnology is an emerging field that focuses on the manipulation and application of materials at the nanometer (nm) scale. One of the fundamental building blocks of nanotechnology is nanoparticles, which have recently gained significant attention across diverse fields, including pharmaceuticals, therapeutic innovations, nanotechnology, and polymer science [1]. Nanoparticles

are defined as solid colloidal particles with sizes ranging from 10 to 1000 nm [2]. Due to their nanoscale dimensions and high surface area-to-volume ratio, nanoparticles exhibit unique physical and chemical properties, making them ideal for various biomedical applications. They can be synthesized using both natural and synthetic polymers; however, natural polymers are often preferred due to their lightweight nature, ease of preparation, and avoidance of organic solvents and high shear forces during synthesis.

Polymers are composed of multiple repeating monomer units. Numerous natural polymers, such as proteins (e.g., collagen, elastin, keratin, and silk fibroin) and polysaccharides (e.g., alginate, chitosan, hyaluronic acid, and cellulose), as well as synthetic polymers (e.g., polylactic acid (PLA), polyvinyl alcohol (PVA), polycaprolactone (PCL), poly(lactic-co-glycolic acid) (PLGA), and polyethylene glycol (PEG)), are widely used in medical applications [3]. It has been demonstrated that natural biopolymers such as chitosan, collagen, and hyaluronic acid (HA) support wound healing, particularly by stimulating anti-inflammatory responses in chronic wounds [4].

Chitosan (CS), a versatile natural biopolymer abundantly available in nature, is widely used for nanoparticle preparation due to its desirable properties, such as low cost, biodegradability, biocompatibility, and non-toxicity [1]. Chitosan is a linear natural polysaccharide derived from the partial deacetylation of chitin under alkaline conditions [5]. Structurally, it consists of β -1,4-linked glucosamine and N-acetylglucosamine residues, offering numerous valuable attributes, including biocompatibility, biodegradability, low toxicity, immune stimulation, mucoadhesive properties, the proton sponge effect, antimicrobial activity, and enhanced bioavailability [6].

CSNPs are commonly synthesized using the ionic gelation method, which is based on electrostatic interactions between oppositely charged ions [7]. Among various ionic gelation approaches, the use of tripolyphosphate (TPP) as a crosslinking agent is the most popular due to its ease of application, low toxicity, and scalability. The size of nanoparticles plays a critical role in determining their biological performance, including biodistribution, stability, drug loading capacity, drug release profile, and toxicity [8]. Moreover, nanoparticle size significantly influences intracellular uptake, transport, and movement in biological fluids [9].

Recent studies have highlighted the promising antimicrobial potential of CSNPs. For instance, Al-Zahrani et al. [10] demonstrated that CSNPs exhibit significant antibacterial activity. Additionally, Pan et al. [57] reported that TPP-loaded CSNPs showed enhanced inhibitory effects against *Escherichia coli* and *Staphylococcus aureus* compared to TPP-free CSNPs. However, the practical use of CSNPs in industrial applications can be challenging due to the high concentrations required, which may not be cost-effective and could induce undesirable changes in the targeted products. To address these limitations, the incorporation of effective antibacterial agents into CSNP formulations has been proposed as a strategy to enhance their antimicrobial efficiency while reducing the required dosage [10].

Antimicrobial peptides (AMPs) have emerged as promising alternatives in the fight against bacterial infections [11]. AMPs are typically positively charged molecules that interact with the negatively charged bacterial membranes, leading to membrane disruption and bacterial cell death [12]. Among AMPs, LL37 is a physiologically relevant, positively charged, amphipathic, α -helical peptide with potent antibacterial properties at a pH of 6 [13]. LL37 exhibits broad-spectrum antimicrobial activity by disrupting bacterial membrane integrity [14]. However, despite its effectiveness, LL37 has several limitations, such as poor stability in biological environments, susceptibility to proteolytic degradation, weak interactions with host macromolecules, and potential toxicity concerns [15]. Encapsulation within suitable delivery systems, such as CSNPs, has been proposed to overcome these challenges and improve the stability and bioactivity of LL37 [16].

In this context, the development of an effective delivery system by loading LL37 onto CSNPs with optimized properties represents a promising strategy for enhancing its antimicrobial potential. Various characterization techniques, including DLS for determining particle size and zeta potential, and Scanning Electron Microscopy (SEM) for morphological analysis, are commonly employed to evaluate the physicochemical properties of CSNPs (1-Agarwal et al., 2018). Chitosan-based

nanoparticles have shown reduced toxicity when used in mucoadhesive formulations [17], further supporting their potential application in biomedical fields such as drug and gene delivery, tissue engineering, bone regeneration, and wound healing [18].

The primary objective of this study is to optimize the formulation of CSNPs by evaluating critical parameters such as chitosan concentration, TPP concentration, chitosan-to-TPP volume ratio, and the effects of additives such as NaCl and Tween 80. The optimized CSNP formulation was then be used for the encapsulation of LL37, followed by an assessment of its encapsulation efficiency, release kinetics, and antibacterial activity. Additionally, the biocompatiblity of the blank and LL37-loaded CSNPs were evaluated and compared to suggest their potential use for biomedical applications.

2. Materials and Methods

2.1. Chemicals and Materials

CS with a low molecular weight and a deacetylation degree of 95% or higher (Sigma Aldrich), TPP (Sigma Aldrich), ultra-pure water, analytical grade acetic acid (AA, glacial, 99%, 5%), Tween 80, NaCl, sodium hydroxide (NaOH), hydrochloric acid (HCl), Dulbecco’s Modified Eagle Medium (DMEM)(Gibco), fetal bovine serum (FBS), gentamicin (Sigma-Aldrich), LL37 peptide (LLGDFFRKSKEKIGKEFKRIVQRIKDFLRNLPVPRTE) (Chinapeptides), Micro BCA Assay Kit (Thermo Scientific), XTT (3-(4,5-dimethylthiazol-2-yl)-2,5-diphenyltetrazolium bromide assay, Sartorius) were purchased, and all chemicals and reagents were used as received.

2.2. Method

2.2.1. Development of CSNPs

Optimization of Development of Blank CSNPs

In the initial stage of the study, solutions containing varying concentrations of CS and sodium TPP were prepared to optimize the nanoparticle formulation. The optimization process aimed to identify the optimal parameters for CSNP production by evaluating different CS:TPP ratios and process conditions. The parameters utilized for CSNP production are summarized in Table 1, providing a comprehensive overview of the experimental design. To facilitate a better understanding of the CSNP production process, a schematic representation is provided in Figure 1, illustrating the key steps involved in the preparation of chitosan nanoparticles via the ionic gelation method.

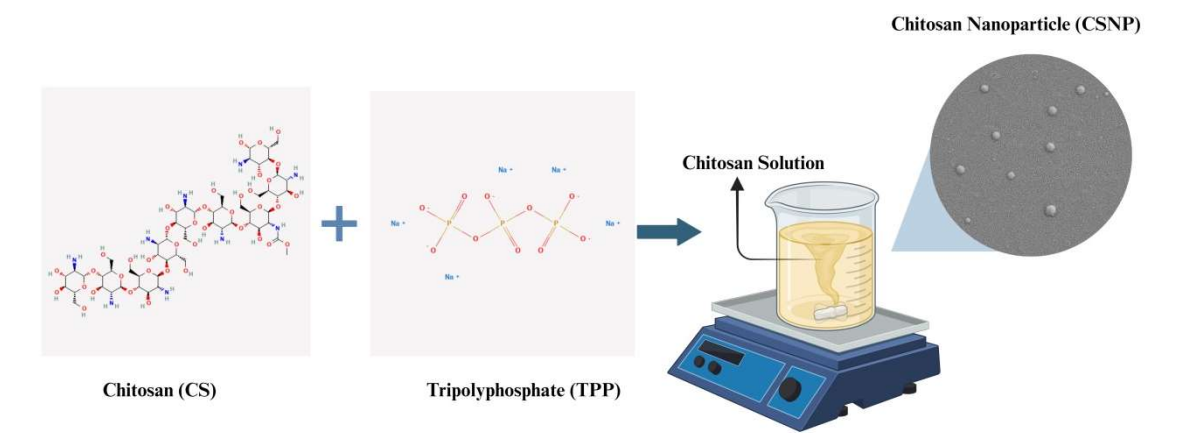


Figure 1. Schematic representation of CSNP production.

Table 1. The parameters utilized for blank CSNP production.

Groups	CS (mg/mL, pH 5)	TPP (mg/mL, pH 2)	CS/TPP (v/v)	NaCl (mM)	Tween80
CSNP-1	0.7	0.3	2:1	-	+
CSNP-2	0.7	0.3	2:1	100	-

CSNP-3	0.3	0.1	2:1	-	+
CSNP-4	0.3	0.1	2:1	100	-

CSNPs (1-4) were produced using variable process medium, and the resulting CSNPs were compared. Firstly, the CS (1% v/v) was dissolved in acetic acid solution, and TPP was dissolved in ultra-pure water for 24 hours. Under room conditions, the volume ratio of CS:TPP (2:1) was added dropwise at a flow rate of 0.25 mL/min and mixed on a magnetic stirrer. The CSNP solution was mixed in a homogenizer (7000 rpm for 2 min) prior to centrifugation. The CSNP solution was centrifuged at 14000 rpm for 40 minutes. For filtration, the solution was filtered sequentially with 0.45 µm and 0.22 µm syringe filters.

Development of LL37-Loaded CSNPs

The optimal nanoparticle (NP) production parameters were determined based on a comparative analysis of the physicochemical characteristics of four CSNP formulations (CSNP-1 to CSNP-4). The CSNP-1 formulation was identified as the most suitable, and its process conditions were selected for further studies. Following the optimization, the production parameters of blank CSNP-1 were utilized for the encapsulation of LL-37 at different concentrations (30, 15, and 7.5 µg/mL). The resulting LL37-loaded CSNP groups were designated as 30-LL37-CSNP, 15-LL37-CSNP, and 7.5-LL37-CSNP, respectively. For nanoparticle preparation, CS at a concentration of 1% (v/v) was dissolved in an acetic acid solution, while TPP was dissolved in ultrapure water. Both solutions were allowed to stir for 24 hours to ensure complete dissolution. After the dissolution period, the LL37 peptide solution was added dropwise to the CS solution at a controlled flow rate of 0.5 mL/min using a syringe pump. The mixture was continuously stirred on a magnetic stirrer for 4 hours at 4°C to promote uniform dispersion. Subsequently, the TPP solution was added dropwise to the CS-LL37 solution at a flow rate of 0.25 mL/min while maintaining a constant stirring condition. The encapsulation process was carried out for an additional 4 hours at a chitosan-to-TPP (CS:TPP) volume ratio of 2:1 (v/v). To enhance nanoparticle homogeneity, the LL37-loaded CSNP solution was subjected to homogenization at 7000 rpm for 2 minutes. Following homogenization, the suspension was centrifuged at 14,000 rpm for 40 minutes to separate the nanoparticles. The supernatants were collected and stored at -20°C for further Micro BCA analysis, while the obtained pellets were lyophilized for long-term storage and subsequent characterization.

2.2.2. Physicochemical Characterization of CSNPs

The particle size, PDI, and ZP of CSNPs were measured using a DLS system (Zetasizer NanoPlus-3, Micromeritics, USA). The mean particle size was determined based on the average of three independent measurements, with each measurement comprising 50 readings. The morphological characteristics of chitosan nanoparticles (CSNPs) were analyzed using a FESEM. The samples were examined under an accelerating voltage of 2 kV to ensure high-resolution imaging.

2.2.3. Encapsulation Efficiency of LL-37 and In-Vitro Release Kinetics

The encapsulation efficiency (EE) of LL37-loaded chitosan nanoparticles (30-LL37-CSNP, 15-LL37-CSNP, and 7.5-LL37-CSNP) was determined using the protein detection assay Micro BCA (Thermo Scientific) and calculated based on equation 1.

$$EE(\%) = \frac{\text{Total LL37 concentration} - \text{LL37 concentration}}{\text{Total LL37 concentration}} * 100 \tag{1}$$

A calibration curve for the Micro BCA assay was established using bovine serum albumin (BSA) as the standard, within a concentration range of 0 to 40 µg/mL, yielding a coefficient of determination R² of 0.9986. All measurements were conducted in triplicate to ensure reproducibility. The formulation that exhibited EE% more than 80 percent were used to conduct the in-vitro LL37 release

measurements. The in vitro release profile of LL37 from CSNP formulations was evaluated by suspending the LL37-CSNPs in phosphate-buffered saline (PBS, pH 6.8) at 37°C. Supernatants were collected at 24-hour intervals over a period of 24 days, and LL37 release was quantified using a calibration curve constructed with the albumin standard in the Micro BCA assay. The calibration curve included standard concentrations of 40, 20, 10, 5, 1, and 0 µg/mL. The encapsulation efficiency was determined based on the LL37 content obtained from this calibration curve.

To characterize the release kinetics of LL37 from CSNPs, the experimental data were fitted to several mathematical models, including zero-order, first-order, Higuchi, Korsmeyer-Peppas, and Hixson-Crowell models. These models provide insights into the drug release mechanism and kinetics. Zero-order kinetics defines the constant release of a drug from a formulation, which is independent of time or concentration; zero-order release is expressed by equation 2, where C_0 is the initial drug concentration, C_t is the amount of drug released at time 't', and K_0 is the zero-order rate constant. Data fitting was performed by plotting the cumulative percentage of drug release against time.

$$C_0 - C_t = K_0 t \quad (2)$$

First Order kinetics describes the drug release occurs exponentially as defined by equation 3, where C_0 is the initial drug concentration, t is time, and K_1 is the first-order rate constant. The obtained data were plotted as the cumulative logarithmic percentage of the remaining drug over time.

$$\text{Log } C = \text{Log } C_0 - \left(\frac{K_t}{2.303} \right) \quad (3)$$

The Korsmeyer-Peppas semi-empirical model predicts drug release mechanisms from polymeric systems and follows equation 4, where C_t / C_∞ represents the fraction (ratio) of drug release at time t , and K is the rate constant. The logarithm of the cumulative drug release percentage was plotted against the logarithm of time.

$$\frac{C_t}{C_\infty} = K t^n \quad (4)$$

The Higuchi model describes drug release from matrix-based systems, where the drug diffusion follows Fick's law. The release kinetics are represented by equation 5, where C_t represents the amount of drug released at time t , and K_H is the Higuchi rate constant. The cumulative percentage of drug release was plotted against the square root of time to evaluate the model's applicability.

$$C_t = K_H \times \sqrt{t} \quad (5)$$

The Hixson-Crowell model describes drug release as being dependent on the surface area and volume of the particles. The mathematical expression for this model is presented as equation 6, where K_H is the rate constant, C_0 is the initial drug concentration, and C_t represents the drug release at time t . The data were fitted by plotting the cube root of the remaining drug percentage against time [19].

$$C_0^{1/3} - C_t^{1/3} = K_H C_t \quad (6)$$

The results were compared across these kinetic models to identify the best fit and to elucidate the potential release mechanisms governing LL37 delivery from the CSNP formulations.

Kinetic models involve mathematical equations that describe the drug release mechanism, and regression analysis is used to fit these models to experimental data. Regression is applied to assess the degree of agreement between the mathematical models and the observed data. Through regression analysis, various statistical metrics such as the coefficient of determination (R^2), Root Mean Square Error (RMSE), Residual Sum of Squares (RSS), Akaike Information Criterion (AIC), and Bayesian Information Criterion (BIC) are calculated for each kinetic model. These metrics are compared to determine the best-fitting model. R^2 indicates how well the model explains the variability in the data and ranges between 0 and 1. A value of 0 means the model does not explain

the data, while a value of 1 indicates a perfect fit. RMSE measures the predictive accuracy of the model; lower RMSE values suggest a better fit. RSS represents the total amount of error in the model's predictions, with smaller values indicating closer alignment with the actual data. AIC evaluates both the goodness of fit and the complexity of the model; among competing models, a lower AIC value generally indicates a better model. BIC is similar to AIC but includes a stronger penalty term for model complexity. Like AIC, BIC is used for model comparison, and lower BIC values indicate a better model fit [20].

2.2.4. Evaluation of In-Vitro Biocompatibility

The in vitro biocompatibility of CSNP formulations was assessed by evaluating their effects on the proliferation of HS2 keratinocyte cells. Initially, HS2 cells were cultured in DMEM supplemented with 10% FBS and antibiotics to ensure optimal growth conditions. To investigate any cytotoxic effects of CSNPs, the cells were exposed to ten different concentrations of CSNPs, ranging from 150 µg/mL to 0.29 µg/mL. Control groups were included, consisting of wells designated as cell control (without CSNPs but with cells) and medium control (without cells and CSNPs). Actively proliferating cells, excluding the medium control wells, were seeded in 96-well culture plates at a density of 5000 cells per well in a volume of 50 µL of complete medium. The plates were incubated at 37°C in a humidified 5% CO₂ incubator for 24, 48, and 72 hours to allow cell proliferation. Following the incubation period, the mitochondrial activity of viable cells was assessed using the 3-(4,5-dimethylthiazol-2-yl)-2,5-diphenyl tetrazolium bromide (XTT) assay (Sartorius). The XTT reagent was added to each well and incubated for an additional 4 hours to enable the enzymatic conversion of the tetrazolium salt to a formazan product by metabolically active cells. Absorbance was measured at 490 nm using an ELISA plate reader to determine the percentage of viable cells. The cell viability for each test condition was calculated relative to the control group, where the untreated control cells were considered to represent 100% viability. The effects of both blank and LL37-loaded CSNP formulations on cell proliferation were analyzed and compared by calculating the relative cell viability percentage. This analysis provided insights into the biocompatibility of the CSNP formulations and their potential impact on HS2 keratinocyte cell proliferation.

2.2.5. Evaluation of Antibacterial Activity

The antibacterial activity of CSNP formulations was assessed against both Gram-positive *Staphylococcus aureus* (ATCC 29213) and Gram-negative *Escherichia coli* (ATCC 25922) bacterial strains. Samples from the CSNP groups were prepared by applying 25 µL of each sample (150 µg/mL) onto disk-shaped filter paper. The disks were allowed to air-dry to ensure uniform distribution of the formulation.

For each bacterial strain, three colonies were selected from cultured plates and suspended in 4–5 mL of Mueller Hinton Broth (MHB). The bacterial suspensions were adjusted to a density of 0.5 McFarland standard, corresponding to approximately 5×10^6 CFU/mL. A 96 U-bottomed well microplate was used for the assay, with a final volume of 100 µL per well. The bacterial suspension was inoculated into each well to achieve the desired cell density. The prepared CSNP-coated filter paper discs were placed into the inoculated wells in triplicate to ensure reproducibility. The microplate was incubated at 37°C for 16 hours under appropriate conditions to allow bacterial growth and CSNP interaction. At the end of the incubation period, the filter paper discs were removed from the wells, and bacterial growth was evaluated by measuring the absorbance at 600 nm using an ELISA microplate reader (Thermo Scientific Multiskan Reader). The absorbance values were used to compare the bacterial viability with control group and to assess bacterial viability in the CSNP treated wells. This method provides a quantitative evaluation of the antibacterial properties of CSNPs against clinically relevant bacterial strains, offering insights into their potential applications in antibacterial therapies.

3. Results and Discussion

3.1. Physicochemical Characteristics of CSNPs and LL37-CSNPs

The present study highlights the impact of formulation and process parameters on the physicochemical properties of CSNPs. The findings demonstrate that appropriate CS:TPP ratios, controlled pH conditions, and optimized stirring rates contribute to achieving nanoparticles with desirable size, distribution, and stability characteristics. The experimental results provide valuable insights for the development of stable and effective CSNP formulations. According to Table 2, the average nanoparticle size, PDI and ZP values for CSNP-1 are at optimum values compared to other groups. LL37 loaded CSNP was developed using CSNP-1 parameters to encapsulate LL37.

Table 2. The average particle size, PDI, and ZP values of the groups.

Groups	Mean Particle Size (nm)	PDI	ZP (mV)
CSNP-1	180.40±2.16	0.289±0.00	40.57±1.82
CSNP-2	198.00±4.48	0.259±0.03	43.68±1.40
CSNP-3	291.90±6.65	0.364±0.01	46.26±0.72
CSNP-4	496.40±9.80	0.321±0.00	35.75±0.97
7.5-LL37-CSNP	195.60±3.50	0.257±0.02	19.26±1.39
15-LL37-CSNP	210.90±2.59	0.306±0.02	51.21±0.93

Among the critical parameters influencing the physicochemical properties of CSNPs, the CS:TPP ratio plays a significant role in determining particle size, distribution, and ZP. Increasing the CS: TPP volume ratio correlates with an increase in nanoparticle size, as a higher volume of CS helps to prevent precipitation and agglomeration. However, an excessive CS proportion can lead to larger particles, as reported by Algharib et al. [9]. Based on these findings, a CS:TPP ratio of 2:1 was selected in the present study to ensure optimal nanoparticle stability and size distribution. The primary role of NaCl in the CS and TPP solution mixtures was to enhance control over nanoparticle formation by reducing the rigidity and electrostatic repulsion of CS chains. This results in more compact particle formation, as corroborated by previous studies [21,22]. Additionally, an optimal concentration of NaCl is crucial for achieving colloidal stability and a uniform particle size distribution, whereas excessively high concentrations can impede the CS-TPP interaction. Studies have also shown that ionized salts weaken electrostatic interactions between CS and TPP, further influencing nanoparticle formation [23].

CS concentration is a pivotal factor in determining the physicochemical characteristics of CSNPs. Higher CS concentrations lead to increased intermolecular interactions and crosslinking with TPP, resulting in the formation of larger particles. This size increment is attributed to the presence of hydroxyl (–OH) groups in CS, which facilitate intermolecular hydrogen bonding, and protonated amino (–NH₃⁺) groups, which contribute to electrostatic repulsion [24]. Morphological variations in CSNPs have been observed with changing CS concentrations [9]. Similarly, increasing TPP concentration promotes greater CS-TPP complex formation, potentially leading to particle aggregation, which is a well-documented limitation of CSNP systems [25].

The incorporation of Tween 80 has been identified as an essential factor in preventing nanoparticle aggregation. Studies have demonstrated that the absence of Tween 80 results in failed nanoparticle formation, while its presence enhances stability. However, increasing the concentration of Tween 80 can contribute to larger particle sizes. For instance, CSNP sizes were reported as 148.8±1.1 nm (PDI=0.066) at 0.5% Tween 80 and 177.0±3.2 nm (PDI=0.090) at 1% Tween 80 [1,26] These variations are further influenced by factors such as the molecular weight and degree of deacetylation of CS [27–29].

The method of CSNP preparation significantly affects particle properties, with dropwise addition of CS solution to TPP solution being crucial for controlled nanoparticle formation. The flow

rate and mixing time during this process are critical factors influencing particle size and PDI. Studies indicate that higher flow rates of TPP lead to increased particle size and PDI values, which aligns with the findings of Majedi et al. [30]. The pH of the CS and TPP solutions is another essential environmental factor governing CSNP formation. An acidic medium is necessary to facilitate the solubility of CS and ensure the protonation of amino groups, which promotes effective solvent diffusion and prevents premature aggregation [31]. It has been observed that pH values exceeding 5.5 lead to decreased protonation and increased agglomeration [32]. In this study, the CS solution pH was maintained at 5, while the TPP solution was adjusted to pH 2. An optimal formation pH range of 3.5-4 was employed to achieve the desired nanoparticle characteristics.

The magnetic stirring speed during the CSNP synthesis process significantly affects particle formation. Optimal stirring facilitates the uniform dispersion of TPP in the CS solution, promoting efficient crosslinking and size reduction. However, excessive stirring can eliminate repulsive forces, leading to aggregation [24,33]. In a study by Algharib et al. (9-Algharib et al., 2022), particle sizes of 138.50 ± 0.50 nm at 500 rpm, 67.17 ± 0.77 nm at 1000 rpm, and 105.50 ± 0.50 nm at speeds above 1000 rpm were reported. In this study, a stirring speed of 800 rpm was maintained to achieve the desired nanoparticle size.

The polydispersity index (PDI) is an important parameter used to evaluate particle size distribution in nanoparticle suspensions. A lower PDI indicates uniform particle size distribution, while higher values reflect polydispersity [34]. In the current study, the PDI values for the blank CSNP (1-2-3-4), 7.5-LL37-CSNP and 15-LL37-CSNP groups ranged between 0.2 and 0.4, suggesting a homogeneous and narrow particle size distribution (Table 2). Similar findings were reported by Algharib et al. [9], where an increase in CS concentration correlated with increased PDI values due to higher agglomeration tendencies.

ZP is a key indicator of nanoparticle stability, with values exceeding ± 30 mV considered essential for physical stability [35]. Lazaridou et al. reported ZP values for CSNPs in the range of +37.6 to +40.1 mV [36]. In this study, the ZP values for CSNP (1-2-3-4), 7.5-LL37-CSNP and 15-LL37-CSNP were determined as 40.57, 43.68, 46.26, 35.75, 19.26 and 51.21 mV, respectively. These values exceed the stability threshold, indicating excellent colloidal stability and potential for enhanced cellular uptake due to interactions with negatively charged cell membranes [9]. The morphological characteristics of CSNPs were analyzed using FE-SEM imaging. The formulations containing Tween 80 exhibited a distinctly spherical morphology (Figure 2).



Figure 2. FE-SEM images of a) CSNP-1, b) 7.5-CSNP-4, c) 15-LL37-CSNP.

DLS and Zeta size analyses revealed that blank CSNPs exhibited an average particle size of 180.40 ± 2.16 nm, a zeta potential of $+40.57 \pm 1.82$ mV, and a polydispersity index (PDI) of 0.289. In contrast, 15-LL37-CSNPs demonstrated an increased size of 210.9 ± 2.59 nm with an enhanced zeta potential of $+51.21 \pm 0.93$ mV, indicating improved stability and interaction potential.

3.2. Encapsulation Efficiency

The encapsulation efficiency (%EE) of LL37 within chitosan nanoparticles (CSNPs) was assessed using the Micro BCA protein assay absorbance values at 562 nm. The calculated %EE values, derived from the LL37 standard curve, are summarized in Table 3. Based on the loaded LL37 concentrations,

the %EE values for CSNPs loaded with 30 µg/mL, 15 µg/mL, and 7.5 µg/mL of LL37 were determined to be 55.57%, 80.32%, and 97.81%, respectively.

Table 3. % EE based on the initial LL37 concentration.

LL37 (µg/mL)	EE (%)
30 µg/mL	55.57±11.90
15 µg/mL	80.32±.94
7.5 µg/mL	97.81±2.72

A higher encapsulation efficiency was observed for CSNPs loaded with 15 µg/mL and 7.5 µg/mL of LL37, indicating a more effective incorporation of the peptide at these concentrations. Specifically, the %EE value of 55.57% for CSNPs loaded with 30 µg/mL LL37 suggests that nearly half of the peptide was successfully encapsulated, while the remaining portion remained unencapsulated. In contrast, the encapsulation efficiencies of 80.32% and 97.81% for 15-LL37-CSNP and 7.5-LL37-CSNP formulations, respectively, demonstrate superior loading efficiency at lower LL37 concentrations. The findings of this study are consistent with previously reported values in the literature. Rashki et al. [37] reported an encapsulation efficiency of 86.9% for LL37-loaded CSNPs, which aligns closely with the values obtained for the 15-LL37-CSNP formulation in the present study. Similarly, Nair et al. [19] investigated curcumin-loaded chitosan nanoparticles at different CS:curcumin ratios (5:1, 4:1, and 3:1) and reported encapsulation efficiencies of 80.4%, 80.2%, and 88.4%, respectively, supporting the trends observed in the current findings. Furthermore, Piras et al. [38] reported an encapsulation efficiency of approximately 75% for temporin within CSNPs, further corroborating the efficiency of chitosan as a nanoparticle carrier system. These results underscore the effectiveness of chitosan nanoparticles in encapsulating LL37, with lower loading concentrations yielding higher encapsulation efficiencies. The findings highlight the potential of CSNPs as a promising delivery vehicle for antimicrobial peptides such as LL37, offering controlled release and improved bioavailability.

3.3. *In Vitro* LL37 Release from CSNPs

The drug release profile of CSNPs plays a crucial role in their therapeutic efficacy [39]. The release characteristics are influenced by various physicochemical properties such as particle shape, size, degradation rate, chemical composition, molecular weight, and solubility. Furthermore, interactions between the drug and polymer matrix, as well as potential drug-drug interactions, significantly impact the release behavior [40].

The cumulative release profiles of LL37 from 15-LL37-CSNP and 7.5-LL37-CSNP over a period of 24 days in phosphate-buffered saline (PBS, pH 6.8) at 37°C are presented in Figure 3. At the end of the 24-day period, the cumulative release of LL37 was determined to be 94.39% for 15-LL37-CSNP and 59.86% for 7.5-LL37-CSNP. The release profile exhibited a linear and sustained release pattern up to day 18, after which the remaining LL37 was gradually released between days 18 and 24. The prolonged and incomplete release of LL37 is likely due to strong interactions between LL37 and the chitosan polymer, which hinder its diffusion into the surrounding medium. This phenomenon is consistent with the findings of Tıǧlı and Pulat [41], who reported that 5-fluorouracil was released from chitosan in a sustained manner under *in vitro* conditions, with cumulative release ranging between 29.1% and 60.8% after 17 days, depending on pH variations.

A major challenge associated with the free form of LL37 is its inherent instability and susceptibility to rapid degradation. Encapsulation within CSNPs provides protection against environmental degradation, thus enhancing its stability and ensuring sustained therapeutic action [42–44]. However, the slow-release rate observed in this study may be attributed to the rigid and hydrophobic core of the CSNPs, which restricts the diffusion of LL37 from the nanoparticle matrix. As reported by Li et al. [58], upon exposure to an aqueous environment, the polymer gradually degrades, allowing the encapsulated LL37 to diffuse into the medium over time.

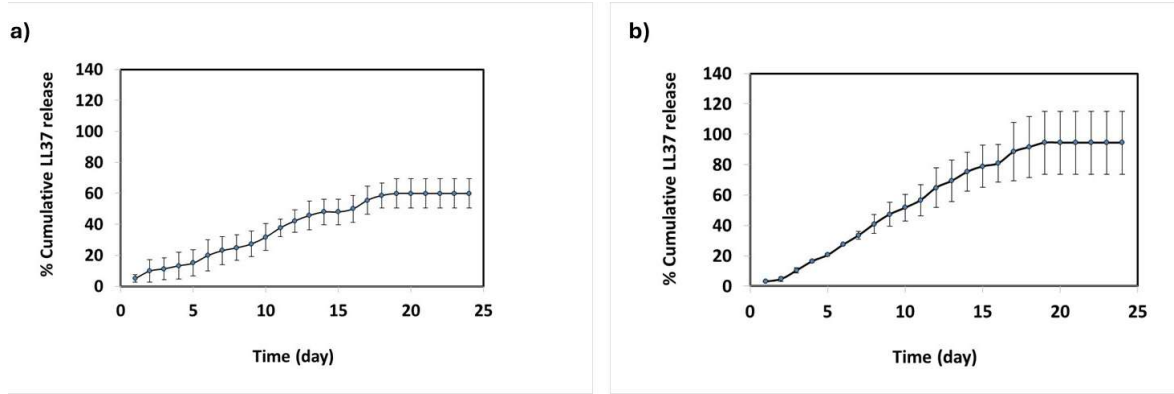


Figure 3. Cumulative release profile of LL37 from a) 7.5-LL37-CSNP and b) 15-LL37-CSNP.

To characterize the release kinetics of LL37 from CSNPs, mathematical models were applied to the experimental data, and the best-fitting model was selected based on the highest correlation coefficient (R^2) and the lowest RMSE, RSS, AIC, and BIC values. As presented in Table 4, the release profiles of both 7.5-LL37-CSNP and 15-LL37-CSNP were best described by the first-order release model. For 7.5-LL37-CSNP, the highest R^2 value was 0.9771, while the lowest RMSE, RSS, AIC, and BIC values were calculated as 2.8708, 197.796, 54.6204, and 56.9765, respectively. Similarly, for 15-LL37-CSNP, the highest R^2 value was 0.9724, with the corresponding lowest RMSE, RSS, AIC, and BIC values calculated as 5.3215, 679.6389, 84.2442, and 86.6003, respectively. These values indicate that the release rate of LL37 is dependent on the remaining amount of the compound, suggesting a delayed yet sustained release process. In first-order release kinetics, the release rate of the active compound is proportional to the remaining drug amount. Therefore, as the amount of drug decreases, the release rate also declines. In the study conducted by Sun et al., 5-FU-loaded chitosan nanoparticles (5-FU-CN) were prepared, and their sustained release behavior was investigated through in vitro release and initial in vivo pharmacokinetic studies. The authors reported that 5-FU-CN followed a first-order kinetic model [45]. Similarly, in the study by Nasri et al., the best-fit kinetic model for microparticles (MPs) was evaluated by determining the highest R^2 value. Overall, the release kinetics of biopeptides from chitosan MPs were found to fit well with the first-order (0.992–0.995) and Korsmeyer–Peppas (0.995–0.996) models [46]. These findings are consistent with the results of the present study.

Table 4. R^2 values for the 24-day release kinetics of 7.5-LL37-CSNP and 15-LL37-CSNP formulations across various models.

7.5-LL37-CSNP						15-LL37-CSNP				
Release kinetics model	R^2	RMSE	RSS	AIC	BIC	R^2	RMSE	RSS	AIC	BIC
First Order Kinetics	0.9771	2.8708	197.7961	54.6204	56.9765	0.9724	5.3215	679.6389	84.2442	86.6003
Korsmeyer Peppas	0.9680	3.3915	276.0563	62.6212	64.9773	0.9616	6.2766	945.5007	92.1679	94.5240
Zero Order Kinetics	0.9569	3.9350	371.6292	69.7562	72.1123	0.9518	7.0313	1186.5542	97.6181	99.9742
Hixson Crowell	0.8958	6.1189	898.5776	90.9462	93.3023	0.8744	11.3493	3091.3721	120.5996	122.9557
Higuchi	0.8760	6.6747	1069.2336	93.1194	94.2975	0.8454	12.5909	3804.7675	123.5830	124.7610

The findings of the present study confirm a logarithmic release profile in which the amount of LL37 released decreases over time as the amount of LL37 remaining within the capsule is reduced, indicating a prolonged release process extending over 24 days. The strong interaction between LL37 and the CSNPs, combined with the rigid nanoparticle core, contributes to the observed slow release kinetics. The encapsulation of LL37 within CSNPs presents a promising strategy to enhance its therapeutic potential by ensuring sustained release and improved stability. The observed release kinetics are consistent with previous literature and further validate the applicability of a first-order release model for predicting CSNP-based drug delivery systems.

3.5. Biocompatibility of CSNPs

An in vitro cell proliferation assay was conducted to assess the any cytotoxic effect of CSNP-1, 7.5-LL37-CSNP and 15-LL37-CSNP on HS2 keratinocyte cells. The cell proliferation graphs for the CSNP-1, 15-LL37-CSNP, and 7.5-LL37-CSNP groups at 24, 48, and 72 hours are presented in Figure 4. The results demonstrate that there was no significant decrease in the HS2 cell viability over a concentration range from 150 $\mu\text{g/mL}$ to 0.29 $\mu\text{g/mL}$ for CSNP-1, 7.5-LL37-CSNPs, and 15-LL37-CSNPs groups at 24, 48, and 72 hours (Figure 4). The cell viability exceeding 70% representing control cell viability can be interpreted as an indication of the suitability of the CSNP groups in facilitating cell proliferation according to the ISO10993-5 standard. The cell proliferation percentages of the CSNP-1, as well as the 7.5-LL37-CSNPs and 15-LL37-CSNPs groups, across 10 different concentrations exceeded 70%, indicating biocompatibility. Similarly, Costa et al. [47] stated that, when compared with control conditions, all tested concentrations of CSNPs were found to be biocompatible with keratinocyte cells, indicating their minimal effect on cellular metabolism. In another study, Piras et al. [38] highlighted the excellent role of loading free temporin onto CS-NPs in reducing the toxicity profile in mammalian cells during cytocompatibility assessment. Similarly, according to the study by Fahimirad et al., the cytotoxic effects of CSLL37NPs on human dermal fibroblast (HDF) cells were evaluated using an MTT assay. The study reported that neither the CSLL37NPs nor the blank CSNPs (at concentrations up to 4096 $\mu\text{g/mL}$) caused a significant reduction in cell viability. In contrast, a notable decrease in cell viability was observed only in cells treated with free LL37 at concentrations higher than 64 $\mu\text{g/mL}$ [44].

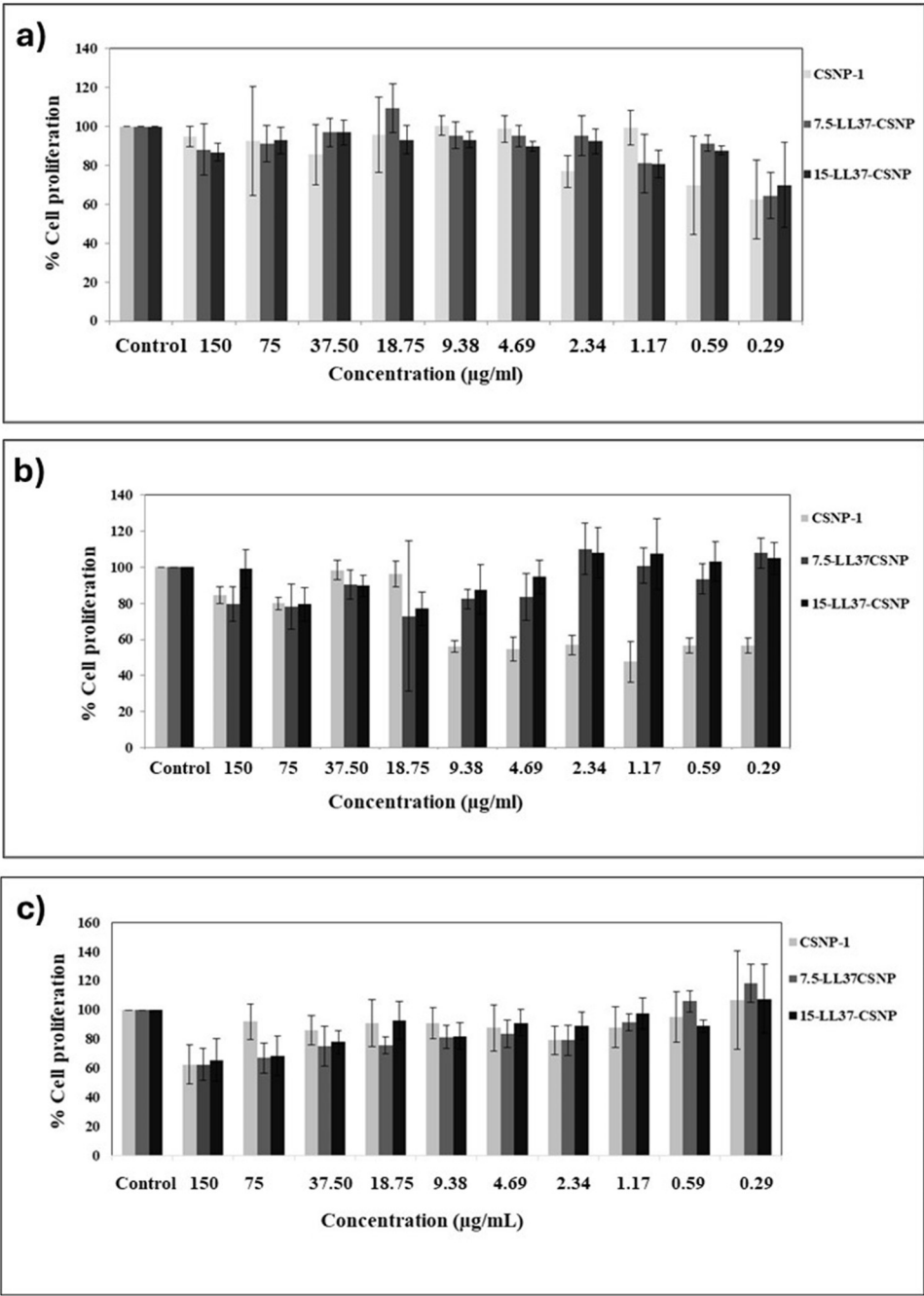


Figure 4. Effects of CSNP formulations on cell proliferations: a) CSNP-1, 7.5-LL37-CSNP and 15-LL37-CSNP at 24 hours, b) CSNP-1, 7.5-LL37-CSNP and 15-LL37-CSNP at 48 hours, c) CSNP-1, 7.5-LL37-CSNP and 15-LL37-CSNP at 72 hours.

Microscopic images corresponding to CSNP-1, 7.5-LL37-CSNP, and 15-LL37-CSNP at 24, 48, and 72 hours (from left to right) are presented in the Figure 5, in comparison to the control group and across different dosages.

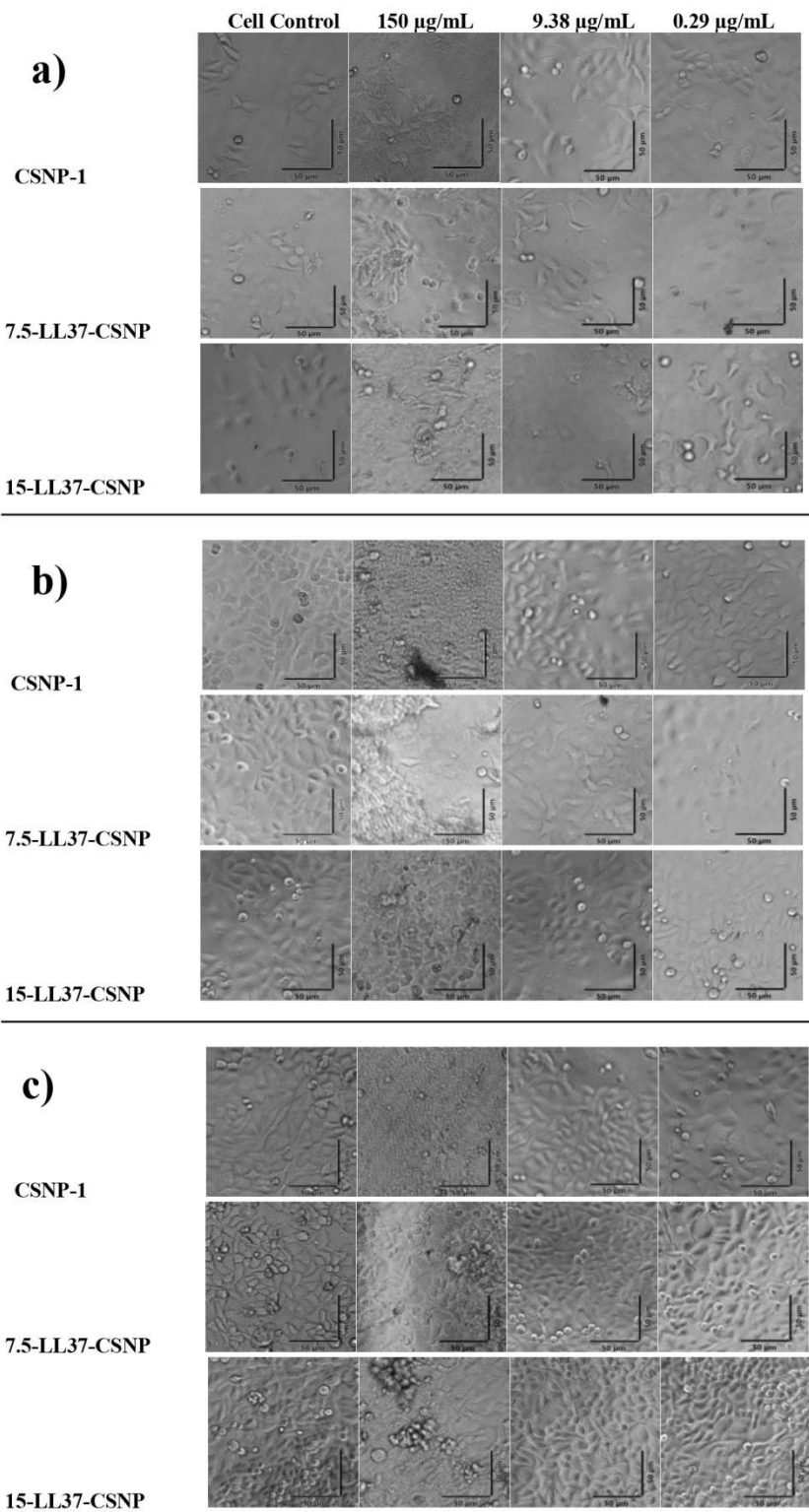


Figure 5. Microscope images of CSNP-1, 7.5-LL37-CSNP and 15-LL37-CSNP after a)24, b)48 and c)72 hours according to HK and different doses.

3.6. Antibacterial Activities of Blank and LL37-CSNPs

The optimal experimental conditions were established to evaluate the antibacterial efficacy of CSNP-1, 15-LL37-CSNP, and 7.5-LL37-CSNP formulations against *E. coli* and *S. aureus* bacterial strains over a 16-hour incubation period. A comparative analysis of CSNP-1, 7.5-LL37-CSNP and 15-LL37-CSNP, as illustrated in Figure 6, demonstrated that both formulations significantly reduced bacterial viability. Notably, the incorporation of LL37 into CSNPs enhanced bactericidal activity

relative to the blank CSNPs, with a more pronounced effect observed against *E. coli*. The antimicrobial efficacy of blank CSNPs is attributed to the intrinsic properties of chitosan, which, in combination with the nanoscale size, provides a high surface area and enhanced interaction with bacterial cells [48,49]. However, despite the observed reduction in bacterial viability with CSNP-1, their antibacterial effect alone was insufficient to achieve the desired efficacy. Therefore, LL37 was incorporated into the CSNP-1 formulation, which exhibited optimal characteristics for enhanced antibacterial activity.

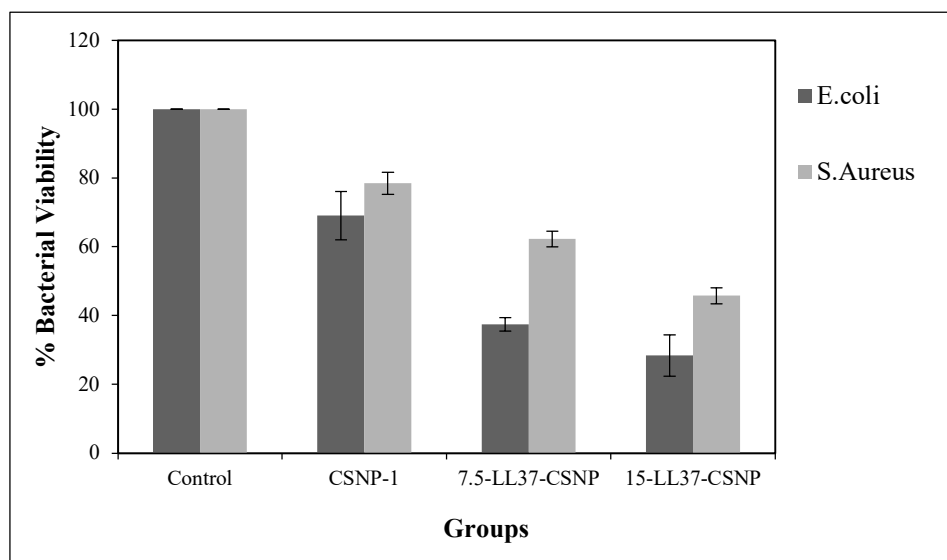


Figure 6. *E. coli* and *S. aureus* viability when treated with CSNP-1, 7.5-LL37-CSNPs and 15-LL37-CSNPs.

It has been confirmed that N-acetylglucosamine, as a monomer unit of chitosan, promotes hemostasis, enhances cell proliferation, and subsequently supports wound healing. All of these properties make CS a strong and promising candidate for the encapsulation of antimicrobial agents as novel nanocarriers for the treatment of microbial infections. Chitosan has also been used as a polymeric vehicle for the delivery of bioactive peptides. Antimicrobial peptides (AMPs) encapsulated in CS nanocarriers have shown successful outcomes in animal models [50–52]. Based on previous reports of in vivo wound healing studies, one of the major challenges associated with the application of free LL37 is the imbalance and rapid degradation at the wound site. Therefore, the desired therapeutic effect requires higher dosages and more frequent administrations. However, the encapsulation of peptides protects them from harsh environmental conditions, thereby reducing their susceptibility to degradation [42,43]. The encapsulation of LL37 within CSNPs can be considered a strategy for enhancing the stability of the AMP. Similarly, Yu et al. (2021) demonstrated that conjugating the antimicrobial peptide microcin J25 (MccJ25) to chitosan nanoparticles resulted in improved stability. In vivo studies have shown that CSLL37NPs lead to more effective healing outcomes and exhibit superior antibacterial performance under in vivo conditions [53]. Another study confirmed that carboxymethyl chitosan nanoparticles loaded with the bioactive peptide OH-CATH30 significantly accelerated wound healing compared to free OH30 or CMCSNPs [54].

Previous studies have demonstrated the potent antimicrobial properties of LL37. For instance, Noore et al. [55] reported that LL37 rapidly eradicates both extracellular and intracellular *S. aureus* compared to conventional antibiotics. Furthermore, Neshani et al. [13] highlighted LL37's broad-spectrum antimicrobial activity, showing lethal effects against *Acinetobacter baumannii*, *Staphylococcus aureus*, *Pseudomonas aeruginosa*, enterococci, and *Escherichia coli*. The findings of this study align with existing literature, suggesting that the antimicrobial mechanisms of LL37-loaded CSNPs extend to both gram-positive and gram-negative bacterial strains.

Comparable studies have also explored the efficacy of chitosan-based nanoparticles for antibacterial applications. Piras et al. [38] reported a 4-log reduction in *Staphylococcus epidermidis*

bacterial counts using temporin loaded CS-NPs over a four-day period compared to CS-NPs alone. Similarly, Almaaytah et al. [56] demonstrated a 5-log reduction in *S. aureus* CFU/mL following treatment with antibacterial short peptide loaded CS-NPs, confirming the potential of such nanoformulations in bacterial eradication.

4. Conclusions

This study provides valuable insights into the production and optimization of CSNPs, examining key parameters such as chitosan and TPP concentrations, CS:TPP volume ratio, flow rate, pH, NaCl solution, Tween 80, sonication, and mixing time, all of which influence particle size within the experimental groups. Notably, the addition of Tween 80 emerged as a critical factor in enhancing nanoparticle stability and preventing aggregation, outperforming NaCl solution in this regard within the CSNP (1-2-3-4) groups. The findings indicate that Tween 80 significantly impacts the average particle size, ZP, and size distribution indices of the CSNPs. In addition, the impact of Tween 80 and NaCl on the physicochemical characteristics of the nanoparticles—such as particle size, polydispersity index (PDI), and surface charge—was examined during the ionic gelation process. Given that these additives can significantly affect nanoparticle stability and morphology, this aspect represents an important technical consideration that has received limited attention in previous studies.

Utilizing the optimal formulation parameters from the CSNP-1 group, LL37-loaded CSNPs were successfully synthesized at concentrations of 30, 15, and 7.5 µg/mL. Encapsulation efficiency analysis revealed that the 7.5-LL37-CSNP and 15-LL37-CSNP samples achieved satisfactory efficiency, making them suitable candidates for further experimental evaluations. This study systematically investigated the relationship between encapsulation efficiency and particle loading capacity by conducting loading experiments at varying LL37 concentrations, ultimately identifying the optimal concentration. Thus, the study offers a unique contribution to the often-neglected issue of 'loading optimization' in the current literature. While the CSNP-1 group demonstrated inherent antimicrobial properties, these effects alone were insufficient to achieve the desired level of efficacy. However, the incorporation of LL37 into the CSNPs significantly enhanced their antimicrobial potential, with the 15-LL37-CSNP group exhibiting superior efficacy compared to the 7.5-LL37-CSNP group. This synergistic combination effectively strengthens the antimicrobial action, rendering the formulation highly effective.

Importantly, the biocompatibility assessment confirmed that both the blank CSNP-1 and the LL37-loaded formulations (7.5-LL37-CSNP and 15-LL37-CSNP) did not exert cytotoxic effects on HS2 cells. This finding, coupled with the successful optimization of nanoparticle sizing, underscores the potential of these formulations for advanced biomedical applications. In conclusion, this study offers novel insights that contribute to the current body of literature by addressing both the improvement of encapsulation efficiency and the optimization of formulation and production parameters. Their promising characteristics position them as viable candidates for drug delivery systems, controlled drug release, and wound healing applications, paving the way for further translational research and clinical exploration.

Author Contributions: Conceptualization, FAZİLET CANATAN ERGÜN and MELTEM DEMİREL KARS; Methodology, FAZİLET CANATAN ERGÜN and GÖKHAN KARS; Validation, GÖKHAN KARS; Investigation, FAZİLET CANATAN ERGÜN; Resources, GÖKHAN KARS; Data curation, FAZİLET CANATAN ERGÜN; Writing—original draft, FAZİLET CANATAN ERGÜN; Writing—review & editing, MELTEM DEMİREL KARS; Visualization, FAZİLET CANATAN ERGÜN; Supervision, MELTEM DEMİREL KARS; Project administration, MELTEM DEMİREL KARS.

Funding: Horizon Europe REGENEU project. No. 101079123

Data Availability Statement: Data is contained within the article.

Acknowledgments: Horizon Europe REGENEU project (No. 101079123) and the Necmettin Erbakan University BAP-221419008 project are acknowledged by authors.

References

- [1] Agarwal, M., Agarwal, M. K., Shrivastav, N., Pandey, S., Das, R., & Gaur, P. (2018). Preparation of chitosan nanoparticles and their in-vitro characterization. *International Journal of Life-Sciences Scientific Research*, 4(2), 1713-1720. DOI:10.21276/ijlssr.2018.4.2.17
- [2] Kreuter J. Nanoparticulate systems for brain delivery of drugs. *J. Adv. Drug. Delivery Revi.*, 2001; 47:65–81. DOI: 10.1016/s0169-409x(00)00122-8
- [3] Vasile, C., Pamfil, D., Stoleru, E., & Baican, M. (2020). New developments in medical applications of hybrid hydrogels containing natural polymers. *Molecules*, 25(7), 1539.
- [4] Thapa, R. K., Diep, D. B., & Tønnesen, H. H. (2020). Topical antimicrobial peptide formulations for wound healing: Current developments and future prospects. *Acta biomaterialia*, 103, 52-67.
- [5] Kahya, N. (2019). Water soluble chitosan derivatives and their biological activities: a review. *Polym. Sci*, 5(1), 1-11. DOI:10.36648/2471-9935.5.1.44
- [6] Algharib, S. A., Dawood, A., Zhou, K., Chen, D., Li, C., Meng, K., ... & Xie, S. (2020). Designing, structural determination and biological effects of rifaximin loaded chitosan-carboxymethyl chitosan nanogel. *Carbohydrate polymers*, 248, 116782. DOI: 10.1016/j.carbpol.2020.116782
- [7] Calvo, P., Remuñan-López, C., Vila-Jato, J. L., & Alonso, M. J. (1997). Chitosan and chitosan/ethylene oxide-propylene oxide block copolymer nanoparticles as novel carriers for proteins and vaccines. *Pharmaceutical research*, 14, 1431-1436. DOI: 10.1023/a:1012128907225
- [8] Algharib, S. A., Dawood, A., & Xie, S. (2020-1). Nanoparticles for treatment of bovine *Staphylococcus aureus* mastitis. *Drug delivery*, 27(1), 292-308. DOI: 10.1080/10717544.2020.1724209
- [9] Algharib, S. A., Dawood, A., Zhou, K., Chen, D., Li, C., Meng, K., ... & Xie, S. (2022). Preparation of chitosan nanoparticles by ionotropic gelation technique: Effects of formulation parameters and in vitro characterization. *Journal of Molecular Structure*, 1252, 132129. DOI:10.1016/j.molstruc.2021.132129
- [10] Al-Zahrani, S. S., Bora, R. S., & Al-Garni, S. M. (2021). Antimicrobial activity of chitosan nanoparticles. *Biotechnology & Biotechnological Equipment*, 35(1), 1874–1880. DOI: 10.1080/13102818.2022.2027816.
- [11] Batoni, G., Maisetta, G., Lisa Brancatisano, F., Esin, S., & Campa, M. (2011). Use of antimicrobial peptides against microbial biofilms: advantages and limits. *Current medicinal chemistry*, 18(2), 256-279. DOI: 10.2174/092986711794088399
- [12] Lei, J., Sun, L., Huang, S., Zhu, C., Li, P., He, J., ... & He, Q. (2019). The antimicrobial peptides and their potential clinical applications. *American journal of translational research*, 11(7), 3919. PMID: 31396309
- [13] Neshani, A., Zare, H., Eidgahi, M. R. A., Kakhki, R. K., Safdari, H., Khaledi, A., & Ghazvini, K. (2019). LL-37: Review of antimicrobial profile against sensitive and antibiotic-resistant human bacterial pathogens. *Gene Reports*, 100519. DOI:10.1016/j.genrep.2019.100519
- [14] Najmi, Z., Kumar, A., Scalia, A. C., Cochis, A., Obradovic, B., Grassi, F. A., ... & Rimondini, L. (2020). Evaluation of nisin and LL-37 antimicrobial peptides as tool to preserve articular cartilage healing in a septic environment. *Frontiers in Bioengineering and Biotechnology*, 8, 561. DOI: 10.3389/fbioe.2020.00561
- [15] Brogden, N. K., & Brogden, K. A. (2011). Will new generations of modified antimicrobial peptides improve their potential as pharmaceuticals?. *International journal of antimicrobial agents*, 38(3), 217-225. DOI: 10.1016/j.ijantimicag.2011.05.004
- [16] Ridyard, K. E., & Overhage, J. (2021). The potential of human peptide LL-37 as an antimicrobial and anti-biofilm agent. *Antibiotics*, 10(6), 650. DOI: 10.3390/antibiotics10060650
- [17] Debnath, S., Kumar, R. S., & Babu, M. N. (2011). Ionotropic gelation—a novel method to prepare chitosan nanoparticles. *Research Journal of Pharmacy and Technology*, 4(4), 492-495.
- [18] Elbehairi, S. E. I., Ismail, L. A., Alfaifi, M. Y., Elshaarawy, R. F., & Hafez, H. S. (2020). Chitosan nano-vehicles as biocompatible delivering tools for a new Ag (I) curcuminoid-Gboxin analog complex in cancer and inflammation therapy. *International Journal of Biological Macromolecules*, 165, 2750-2764. DOI: 10.1016/j.ijbiomac.2020.10.153

19. [19] Nair, R. S., Morris, A., Billa, N., & Leong, C. O. (2019). An evaluation of curcumin-encapsulated chitosan nanoparticles for transdermal delivery. *Aaps Pharmscitech*, 20(2), 69. DOI: 10.1208/s12249-018-1279-6
20. [20] Costa, P., & Lobo, J. M. S. (2001). Modeling and comparison of dissolution profiles. *European journal of pharmaceutical sciences*, 13(2), 123-133.
21. [21] Sreekumar, S., Goycoolea, F. M., Moerschbacher, B. M., & Rivera-Rodriguez, G. R. (2018). Parameters influencing the size of chitosan-TPP nano-and microparticles. *Scientific reports*, 8(1), 4695. DOI: 10.1038/s41598-018-23064-4
22. [22] Antoniou, J., Liu, F., Majeed, H., Qi, J., Yokoyama, W., & Zhong, F. (2015). Physicochemical and morphological properties of size-controlled chitosan-tripolyphosphate nanoparticles. *Colloids and Surfaces A: Physicochemical and Engineering Aspects*, 465, 137-146. DOI:10.1016/j.colsurfa.2014.10.040
23. [23] Huang, Y., & Lapitsky, Y. (2011). Monovalent salt enhances colloidal stability during the formation of chitosan/tripolyphosphate microgels. *Langmuir*, 27(17), 10392-10399. DOI: 10.1021/la201194a
24. [24] Fan, W., Yan, W., Xu, Z., & Ni, H. (2012). Formation mechanism of monodisperse, low molecular weight chitosan nanoparticles by ionic gelation technique. *Colloids and surfaces B: Biointerfaces*, 90, 21-27. DOI: 10.1016/j.colsurfb.2011.09.042
25. [25] Bangun, H., Tandiono, S., & Arianto, A. (2018). Preparation and evaluation of chitosan-tripolyphosphate nanoparticles suspension as an antibacterial agent. *Journal of Applied Pharmaceutical Science*, 8(12), 147-156. DOI: 10.7324/JAPS.2018.81217
26. [26] Ozturk, K., Arslan, F. B., Tavukcuoglu, E., Esendagli, G., & Calis, S. (2020). Aggregation of chitosan nanoparticles in cell culture: Reasons and resolutions. *International Journal of Pharmaceutics*, 578, 119119. DOI: 10.1016/j.ijpharm.2020.119119
27. [27] Gan, Q., Wang, T., Cochrane, C., & McCarron, P. (2005). Modulation of surface charge, particle size and morphological properties of chitosan-TPP nanoparticles intended for gene delivery. *Colloids and Surfaces B: Biointerfaces*, 44(2-3), 65-73. DOI: 10.1016/j.colsurfb.2005.06.001
28. [28] Zhao, J., & Wu, J. (2006). Preparation and characterization of the fluorescent chitosan nanoparticle probe. *Chinese Journal of Analytical Chemistry*, 34(11), 1555-1559. DOI:10.1016/S1872-2040(07)60015-2
29. [29] Csaba, N., Köping-Höggård, M., & Alonso, M. J. (2009). Ionically crosslinked chitosan/tripolyphosphate nanoparticles for oligonucleotide and plasmid DNA delivery. *International journal of pharmaceutics*, 382(1-2), 205-214. DOI: 10.1016/j.ijpharm.2009.07.028
30. [30] Majedi, F. S., Hasani-Sadrabadi, M. M., VanDersarl, J. J., Mokarram, N., Hojjati-Emami, S., Dashtimoghadam, E., ... & Renaud, P. (2014). On-chip fabrication of paclitaxel-loaded chitosan nanoparticles for cancer therapeutics. *Advanced Functional Materials*, 24(4), 432-441. DOI: 10.1002/adfm.201301628
31. [31] Pilipenko, I., Korzhikov-Vlakh, V., Sharoyko, V., Zhang, N., Schäfer-Korting, M., Rühl, E., ... & Tennikova, T. (2019). pH-sensitive chitosan-heparin nanoparticles for effective delivery of genetic drugs into epithelial cells. *Pharmaceutics*, 11(7), 317. DOI: 10.3390/pharmaceutics11070317
32. [32] Hussain, Z., and S. Sahudin. "Preparation, Characterisation and Colloidal Stability of Chitosan-Tripolyphosphate Nanoparticles: Optimisation of Formulation and Process Parameters". *International Journal of Pharmacy and Pharmaceutical Sciences*, vol. 8, no. 3, Mar.2016, pp. 297-08.
33. [33] Jonassen, H., Kjoniksen, A. L., & Hiorth, M. (2012). Stability of chitosan nanoparticles cross-linked with tripolyphosphate. *Biomacromolecules*, 13(11), 3747-3756. DOI: 10.1021/bm301207a
34. [34] Hassan, A., Sahudin, S., Hussain, Z., Hussain, M., & Hussain, M. (2018). Self-assembled chitosan nanoparticles for percutaneous delivery of caffeine: Preparation, characterization and in vitro release studies. *Int J App Pharm*, 10(4), 172-185.
35. [35] Nallamuthu, I., Devi, A., & Khanum, F. (2015). Chlorogenic acid loaded chitosan nanoparticles with sustained release property, retained antioxidant activity and enhanced bioavailability. *Asian journal of pharmaceutical sciences*, 10(3), 203-211. DOI:10.1016/j.ajps.2014.09.005
36. [36] Lazaridou, M., Christodoulou, E., Nerantzaki, M., Kostoglou, M., Lambropoulou, D. A., Katsarou, A., ... & Bikiaris, D. N. (2020). Formulation and in-vitro characterization of chitosan-nanoparticles loaded with

- the iron chelator deferoxamine mesylate (DFO). *Pharmaceutics*, 12(3), 238. DOI: 10.3390/pharmaceutics12030238
37. [37] Rashki, S., Safardoust-Hojaghan, H., Mirzaei, H., Abdulsahib, W. K., Mahdi, M. A., Salavati-Niasari, M., ... & Mousavi, S. G. A. (2022). Delivery LL37 by chitosan nanoparticles for enhanced antibacterial and antibiofilm efficacy. *Carbohydrate Polymers*, 291, 119634. DOI: 10.1016/j.carbpol.2022.119634
 38. [38] Piras, A. M., Maisetta, G., Sandreschi, S., Gazzarri, M., Bartoli, C., Grassi, L., ... & Batoni, G. (2015). Chitosan nanoparticles loaded with the antimicrobial peptide temporin B exert a long-term antibacterial activity in vitro against clinical isolates of *Staphylococcus epidermidis*. *Frontiers in microbiology*, 6, 372. DOI: 10.3389/fmicb.2015.00372
 39. [39] Herdiana, Y., Wathoni, N., Shamsuddin, S., & Muchtaridi, M. (2022). Drug release study of the chitosan-based nanoparticles. *Heliyon*, 8(1). DOI: 10.1016/j.heliyon.2021.e08674
 40. [40] Iacob, A. T., Lupascu, F. G., Apotrosoaei, M., Vasincu, I. M., Tauser, R. G., Lupascu, D., ... & Profire, L. (2021). Recent biomedical approaches for chitosan based materials as drug delivery nanocarriers. *Pharmaceutics*, 13(4), 587. DOI: 10.3390/pharmaceutics13040587
 41. [41] Tıǧlı Aydın, R. S., & Pulat, M. (2012). 5-Fluorouracil encapsulated chitosan nanoparticles for pH-stimulated drug delivery: Evaluation of controlled release kinetics. *Journal of Nanomaterials*, 2012(1), 313961. DOI: 10.1155/2012/313961
 42. [42] Lin, X., Wang, R., & Mai, S. (2020). Advances in delivery systems for the therapeutic application of LL37. *Journal of Drug Delivery Science and Technology*, 60, 102016.
 43. [43] Ramos, R., Silva, J. P., Rodrigues, A. C., Costa, R., Guardão, L., Schmitt, F., ... & Gama, M. (2011). Wound healing activity of the human antimicrobial peptide LL37. *Peptides*, 32(7), 1469-1476. DOI: 10.1016/j.peptides.2011.06.005
 44. [44] Fahimirad, S., Ghaznavi-Rad, E., Abtahi, H., & Sarlak, N. (2021). Antimicrobial activity, stability and wound healing performances of chitosan nanoparticles loaded recombinant LL37 antimicrobial peptide. *International journal of peptide research and therapeutics*, 27(4), 2505-2515. DOI: 10.1007/s10989-021-10268-y
 45. [45] Sun, L., Chen, Y., Zhou, Y., Guo, D., Fan, Y., Guo, F., ... & Chen, W. (2017). Preparation of 5-fluorouracil-loaded chitosan nanoparticles and study of the sustained release in vitro and in vivo. *Asian journal of pharmaceutical sciences*, 12(5), 418-423.
 46. [46] Nasri, R., Hamdi, M., Touir, S., Li, S., Karra-Chaâbouni, M., & Nasri, M. (2021). Development of delivery system based on marine chitosan: Encapsulation and release kinetic study of antioxidant peptides from chitosan microparticle. *International Journal of Biological Macromolecules*, 167, 1445-1451.
 47. [47] Costa, E. M., Silva, S., & Pintado, M. (2023). Chitosan nanoparticles production: optimization of physical parameters, biochemical characterization, and stability upon storage. *Applied Sciences*, 13(3), 1900. DOI:10.3390/app13031900
 48. [48] Shukla, S. K., Mishra, A. K., Arotiba, O. A., & Mamba, B. B. (2013). Chitosan-based nanomaterials: A state-of-the-art review. *International journal of biological macromolecules*, 59, 46-58. DOI: 10.1016/j.ijbiomac.2013.04.043
 49. [49] Ing, L. Y., Zin, N. M., Sarwar, A., & Katas, H. (2012). Antifungal activity of chitosan nanoparticles and correlation with their physical properties. *International journal of Biomaterials*, 2012(1), 632698. DOI: 10.1155/2012/632698
 50. [50] Patrulea, V., Ostafe, V., Borchard, G., & Jordan, O. (2015). Chitosan as a starting material for wound healing applications. *European Journal of Pharmaceutics and Biopharmaceutics*, 97, 417-426.
 51. [51] Keong, L. C., & Halim, A. S. (2009). In vitro models in biocompatibility assessment for biomedical-grade chitosan derivatives in wound management. *International journal of molecular sciences*, 10(3), 1300-1313.
 52. [52] Fahimirad, S., Ajallouei, F., & Ghorbanpour, M. (2019). Synthesis and therapeutic potential of silver nanomaterials derived from plant extracts. *Ecotoxicology and environmental safety*, 168, 260-278.
 53. [53] Yu, H., Ma, Z., Meng, S., Qiao, S., Zeng, X., Tong, Z., & Jeong, K. C. (2021). A novel nanohybrid antimicrobial based on chitosan nanoparticles and antimicrobial peptide microcin J25 with low toxicity. *Carbohydrate Polymers*, 253, 117309.

54. [54] Sun, T., Zhan, B., Zhang, W., Qin, D., Xia, G., Zhang, H., ... & Lee, W. H. (2018). Carboxymethyl chitosan nanoparticles loaded with bioactive peptide OH-CATH30 benefit nonscar wound healing. *International journal of nanomedicine*, 5771-5786.
55. [55] Noore, J., Noore, A., & Li, B. (2013). Cationic antimicrobial peptide LL-37 is effective against both extra- and intracellular *Staphylococcus aureus*. *Antimicrobial agents and chemotherapy*, 57(3), 1283-1290. DOI: 10.1128/aac.01650-12
56. [56] Almaaytah, A., Mohammed, G. K., Abualhajjaa, A., & Al-Balas, Q. (2017). Development of novel ultrashort antimicrobial peptide nanoparticles with potent antimicrobial and antibiofilm activities against multidrug-resistant bacteria. *Drug design, development and therapy*, 3159-3170. DOI: 10.2147/DDDT.S147450
57. [57] Pan, C., Qian, J., Fan, J., Guo, H., Gou, L., Yang, H., & Liang, C. (2019). Preparation nanoparticle by ionic cross-linked emulsified chitosan and its antibacterial activity. *Colloids and Surfaces A: Physicochemical and Engineering Aspects*, 568, 362-370. DOI: 10.1016/j.colsurfa.2019.02.039
58. [58] Li, F., Jin, H., Xiao, J., Yin, X., Liu, X., Li, D., & Huang, Q. (2018). The simultaneous loading of catechin and quercetin on chitosan-based nanoparticles as effective antioxidant and antibacterial agent. *Food research international*, 111, 351-360. DOI: 10.1016/j.foodres.2018.05.038

Disclaimer/Publisher's Note: The statements, opinions and data contained in all publications are solely those of the individual author(s) and contributor(s) and not of MDPI and/or the editor(s). MDPI and/or the editor(s) disclaim responsibility for any injury to people or property resulting from any ideas, methods, instructions or products referred to in the content.